Title

A Size Threshold for Enhanced Magnetoresistance in Colloidally Prepared CoFe2O4 Nanoparticle Solids.

Journal

ACS Central Science, 4(9)

ISSN

2374-7943

Authors

Zhou, Benjamin

Rinehart, Jeffrey

Publication Date

2018-09-26

DOI

10.1021/acscentsci.8b00399

Peer reviewed

ACS central science

Research Article

Cite This: ACS Cent. Sci. 2018, 4, 1222−1227

http://pubs.acs.org/journal/acscii

A Size Threshold for Enhanced Magnetoresistance in Colloidally Prepared $CoFe_2O_4$ Nanoparticle Solids

Benjamin H. Zhou[†] and Jeffrey D. Rinehart*[,†,‡]

[†]Materials Science and Engineering Program and [‡]Department of Chemistry and Biochemistry, University of California—San Diego, La Jolla, California 92093, United States

Supporting Information

ABSTRACT: The phenomenon of granular magnetoresistance offers the promise of rapid functional materials discovery and high-sensitivity, low-cost sensing technology. Since its discovery over 25 years ago, a major challenge has been the preparation of solids composed of well-characterized, uniform, nanoscale magnetic domains. Rapid advances in colloidal nanochemistry now facilitate the study of more complex and finely controlled materials, enabling the rigorous exploration of the fundamental nature and maximal capabilities of this intriguing class of spintronic materials. We present the first study of size-dependence in granular magnetoresistance using colloidal nanoparticles. These data demonstrate a strongly nonlinear size-dependent magnetoresistance with smaller particles having strong $\Delta R/R \sim 18\%$ at 300 K and larger particles showing a 3-fold decline. Importantly, this indicates that $CoFe_2O_4$ can act as an effective room temperature granular magnetoresistor and that neither a high superparamagnetic blocking temperature nor a low overall resistance are determining factors in viable magnetoresistance values for sensing applications. These results demonstrate the promise of wider exploration of nontraditional granular structures composed of nanomaterials, molecule-based magnets, and metal-organic frameworks.

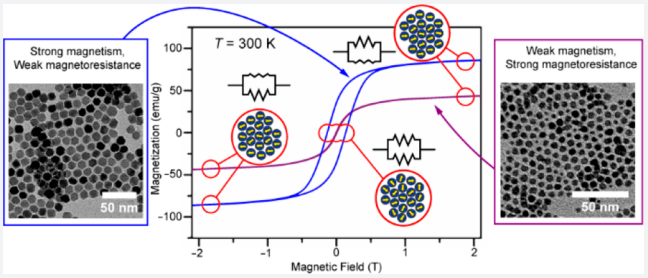

Controlling the flow of electrons by switching magnetization was one of the most impactful advancements of the digital revolution. In particular, the discovery of giant magnetoresistance (GMR) led to the first commercial applications of spintronic technology nearly 40 years ago.[1,2] From its initial use in hard drive read-heads, a continuous stream of advances in giant (GMR), tunnelling (TMR), anisotropic (AMR), and other forms of MR have led to smaller, faster, and more sensitive electrical detection. Although reading and writing digital data remains a main driver of MR research, other detection platforms where speed and sensitivity are important have also become prominent. These technologies include navigation,[3−5] biochemical and chemical detection,[6−8] magnetic relaxometry,[9,10] and nondestructive materials testing.[11−13]

One method to improve the sensitivity of an MR-based sensor is to increase the number of magnetic layers traversed by an electron moving through the device. The magnetization of these layers can be either maximally aligned to enhance the current or antialigned to impede it. In commercial devices, this can be done by deposition of multilayer thin-film devices of increasingly complex architecture. Very early on in the development of MR devices, an alternative geometry was proposed wherein small-grain bulk materials would be pressed together, or bulk mixtures would be phase-separated into small magnetic domains surrounded by conducting or insulating material.[14,15] Ideally in this geometry, each magnetic grain boundary can be a spin-selecting junction, and the total number of junctions is increased by many orders of magnitude. With simple device preparation, minimal materials cost, and low equipment investment, such an architecture could rapidly expand the scope and viability of MR sensing devices. Although early formulations suffered from poor grain boundaries and size distributions, advances in colloidal nanoparticle synthesis over the past few decades now allow many types of nanoparticles to be chemically synthesized as free-standing particles with tight control over size, morphology, and surface chemistry. This developing synthetic control has led to a re-examining of the viability of granular magnetoresistance via a bottom-up nanochemistry approach.

Overwhelmingly, the most studied material to date is the ferrimagnetic inverse spinel Fe_3O_4 (magnetite). Ease of synthesis, stability, strong magnetization, and predicted half-metallicity with full spin polarization have all contributed to the prevalence of Fe_3O_4 nanoparticle composites as research MR materials. Recent work on granular MR in Fe_3O_4 has demonstrated its promise by increasing differential magnetoresistance

$$\frac{\Delta R}{R} = -\frac{R_H - R_{H_c}}{R_{H_c}} \times 100\% \quad (1)$$

from 1.2% (ΔH = 450 mT)[17] to values exceeding 20% at equivalent ΔH.[18] It should be noted that by this definition a perfect magnetoresistor will have $\Delta R/R$ = 100% instead of

Received: June 26, 2018
Published: August 22, 2018

DOI: 10.1021/acscentsci.8b00399
ACS Cent. Sci. 2018, 4, 1222−1227

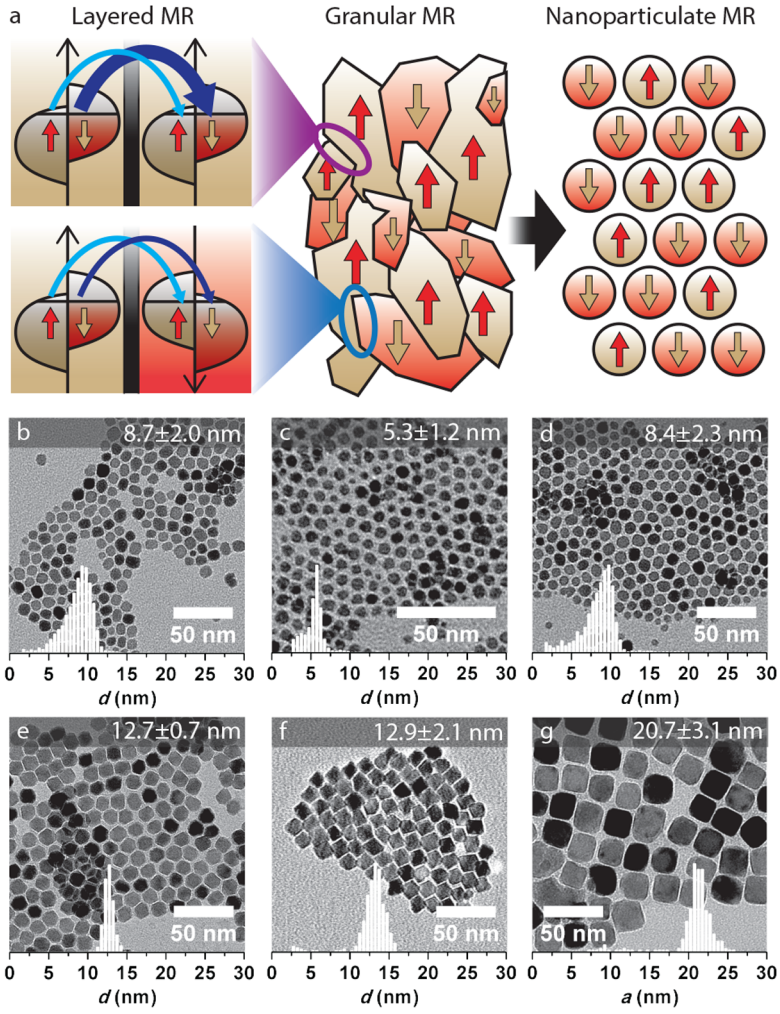

Figure 1. (a) Scheme of the evolution of MR from single-junction thin-film devices to multijunction granular materials to multijunction nanoparticulate materials with exquisite control over grain properties. Transmission electron micrographs and size distribution histograms of (b) Fe_3O_4 and (c–g) $CoFe_2O_4$ nanoparticles used in this study. The diameter d in parts b–f was calculated from the projected area A ($d = \sqrt{4A/\pi}$) while the side length a in part g was calculated as $a = \sqrt{A}$.[16]

approaching infinity, as in definitions that divide by the lower value of the resistance (Figure S1). This empirical evidence suggests that nanostructuring is capable of transforming granular MR from a curiosity into a viable technology; however, from a synthetic chemistry perspective, only the barest surface of the materials parameter space has been explored.[17−28]

Magnetic properties such as coercivity, saturation magnetization, and remanent magnetization are strongly size-dependent in nanomaterials of d = 1−20 nm, yet a study on the MR of well-defined, colloidally prepared materials is lacking from the literature. In this work we perform the first such study using nanoparticles of $CoFe_2O_4$. The greater anisotropy of $CoFe_2O_4$ compared to Fe_3O_4 has been used to enhance the MR properties of Fe_3O_4 through doping[29] and exchange coupling,[30,31] but the MR of stoichiometric $CoFe_2O_4$ alone has not been studied. Intriguingly, we find that single-domain ferrimagnetism or even blocked superparamagnetism is unnecessary to observe viable MR at 300 K; the most important factor is nanoparticle size.

Nanoparticles in this work were synthesized according to literature heat-up processes involving the thermal decomposition of Fe(III) and Co(II) acetylacetonate salts in the presence of oleic acid and oleylamine in high-boiling-point solvents.[32,33] Transmission electron microscopy (TEM) statistics were used to verify consistent size and shape for five separate synthetic preparations of $CoFe_2O_4$ (d = 5.3, 8.4, 12.7, 12.9, 20.7 nm) (Figure 1b–f) as well as an Fe_3O_4 sample (d = 8.7 nm) for comparison. Smaller nanoparticles (d = 5–9 nm) were roughly spherical in shape, and larger nanoparticles exhibited some faceting due to growth along preferential crystalline faces. The d = 12.7 nm and d = 12.9 nm samples showed polyhedral shapes, while convex cubes are observed for the d = 20.7 nm sample. Of particular note are d = 12.9 nm $CoFe_2O_4$ nanoparticles (Figure 1e), which took truncated octahedral forms allowing them to self-assemble into semi-regular lattices. Powder-averaged X-ray diffraction (pXRD) confirmed the inverse spinel crystal structure of AB_2O_4 ferrites for all samples (Figure S2).

As-synthesized nanoparticles form stable colloidal suspensions in nonpolar solvents due to the presence of long-chain ligands such as oleic acid and oleylamine. Ligand exchange of the native long-chain ligands to the small inorganic BF_4^- ion was performed according to a literature procedure[34] in order to

DOI: 10.1021/acscentsci.8b00399
ACS Cent. Sci. 2018, 4, 1222−1227

improve the conductivity of the final nanoparticle pellets. Although significant work has been done to improve conductivity and even control spin-transport through ligand design,[19,20,28] in this work we focus on high-temperature properties, and simply decreasing interparticle distance was sufficient to achieve viable conductivity. The removal of the hydrophobic ligands was evident from the ability to disperse ligand-exchanged nanoparticles in polar solvents such as dimethylformamide. TEM also demonstrates a reduced interparticle spacing in self-assembled layers cast from the BF_4^--exchanged nanoparticles, compared to the TEM of the nanoparticles with their original ligands (Figure S3).

In the nanoregime, magnetic properties become strongly size-dependent as the particle transitions from multidomain to single-domain to superparamagnetic behavior. To characterize the properties of each particle sample, the temperature-dependence of the magnetic moment was examined. Initially, samples were cooled to T = 5 K in the absence of a magnetic field and subsequently subjected to a small field of H = 100 Oe. For samples of all particle diameters, these zero-field-cooled (ZFC) samples are unable to magnetize due to the large thermal barrier to reorienting their magnetic moments. As temperature is raised, the magnetic moment becomes able to freely respond to the external field at its blocking temperature (T_B), reaching a magnetic moment equivalent to that of a sample that was cooled under field-cooled (FC) conditions. As expected, T_B is a function of d, with only $CoFe_2O_4$ (d = 5.3 nm) and Fe_3O_4 (d = 8.7 nm) becoming unblocked below T = 300 K (Figure 2, Figure S3). To determine the saturation magnetization (M_s) and coercive field (H_c) of each sample, moment vs field scans were collected from −7 to 7 T at 300 K. Again, the expected size-dependence is observed, with larger particles displaying stronger H_c and higher M_s. These results confirm that all samples are within the superparamagnetic regime (Table S1).

With a structurally and magnetically characterized array of particle sizes, each material was then tested for magneto-resistive properties. For these measurements, pressed pellets of each sample were electrically contacted and subjected to a variable magnetic field (Figure 3a). At 300 K, $CoFe_2O_4$ (d = 5.3 nm) was biased under H = −7 T, and its resistance (R) was monitored as a function of increasing magnetic field. At large negative fields, the resistance is only weakly dependent on field, yet as H approaches 0 T, the resistance rapidly increases, reaching a maximum value only after reaching H_c. Since $CoFe_2O_4$ is an unblocked superparamagnet at 300 K, H_c = 0 T. This behavior is consistent with minimal resistance at maximum spin alignment ($M = M_s$) and maximum resistance at minimal spin alignment (M = 0; $H = H_c$, Figure S4). When field is scanned in the reverse direction (7 to −7 T), the resistance values are mirrored across the y-axis. When subjected to the maximum magnetic field, $CoFe_2O_4$ (d = 5.3 nm) exhibits $\Delta R/R$ = 19.2%. These results indicate that the MR mechanism at work here does not necessitate ordered magnetism. In fact, since T_B = 175 K for these particles, MR does not even require blocked superparamagnetism. By comparison, Fe_3O_4 (d = 8.7 nm) in an equivalent sample and electrode configuration results in $\Delta R/R$ = 10%, despite significantly higher magnetization values (Figure S5).

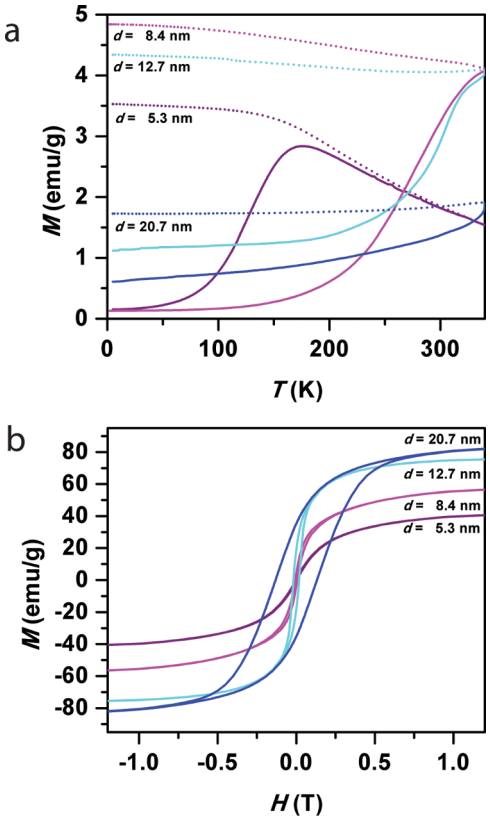

Figure 2. (a) Plots of magnetic moment vs temperature under zero-field-cooled (ZFC, solid lines) and field-cooled (FC, dashed lines) conditions with an applied field of 100 Oe. (b) Field-dependence of the magnetic moment of $CoFe_2O_4$ nanoparticles measured at 300 K.

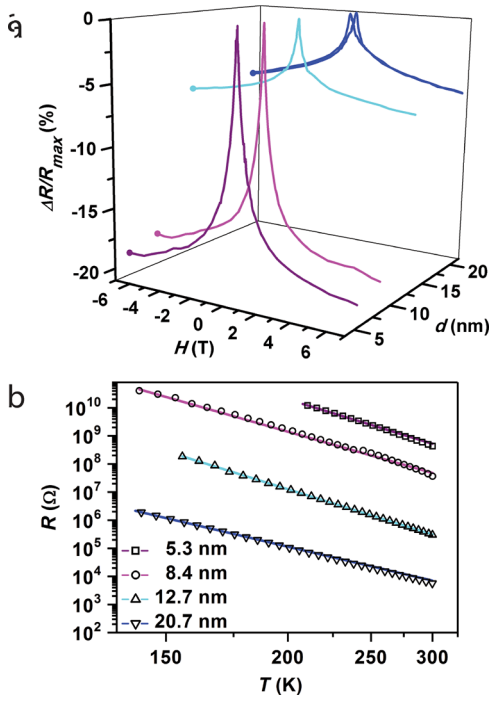

Figure 3. (a) $CoFe_2O_4$ magnetoresistance at 300 K as a function of magnetic field, H, and particle diameter, d. The split peaks observed for d = 20.7 nm are a result of magnetic hysteresis (Figure S4). (b) Temperature-dependent resistance of $CoFe_2O_4$ nanoparticle pellets without an applied magnetic field. Symbols represent measured data points while colored lines are fits based on eq 2.

DOI: 10.1021/acscentsci.8b00399
ACS Cent. Sci. 2018, 4, 1222−1227

To study the effect of increasing particle size on the MR, $CoFe_2O_4$ (d = 8.4, 12.7, 20.7 nm) was tested as well. Each sample displays progressively higher M_s, H_c, and T_B values as expected for superparamagnets with more spin centers, yet a contrasting trend was observed in their MR. $CoFe_2O_4$ (d = 8.4 nm) possesses similar MR ($\Delta R/R$ = 18.4%) to $CoFe_2O_4$ (d = 5.3 nm) despite an enhancement in M_s of over 25%. Surprisingly, this seems to indicate an inherent granular MR value that is inert to size-based effects. When size is further increased, however, a precipitous drop in MR is observed with $\Delta R/R$ = 6.6% and 6.1% for $CoFe_2O_4$ (d = 12.7 nm) and $CoFe_2O_4$ (d = 20.7 nm), respectively. One possible explanation for this behavior is that the 5.3 and 8.4 nm nanoparticles have significantly lower H_c than the 12.7 and 20.7 nm nanoparticles. Coercive granular samples have been predicted to show a decreased magnetoresistance due to decreased ability to break alignment with the anisotropy axis and align with the magnetic field.[35] However, magnetoresistance curves taken at 175 K, where all four nanoparticle samples are blocked, show the same trend in $\Delta R/R$ (Figure S6), and it is clear from the M vs H data that the external field is able to magnetize the sample in all cases. Another possibility is that spin polarization increases as the nanoparticle size decreases. This is consistent with a smaller carrier concentration and shorter distances for electrons to travel between grain interfaces.

Further insight into the charge transport mechanism in these samples can be gleaned from the temperature-dependence of the resistance (Figure 3b). The zero-field resistance of each $CoFe_2O_4$ sample was measured between 300 K and a lower bound dictated by the instrumentation and sample quality. Within the measured regime, all $CoFe_2O_4$ samples displayed a linear relationship between ln R and $T^{-0.5}$, where R and T are resistance and temperature, respectively. This linear relationship indicates that electrical conductivity occurs via tunnelling of charge carriers between nanoparticles.[35,36] Although exact resistivity values were only obtained for two samples due to sample fragility, the measured resistance values scale similarly due to roughly similar sample geometry. These values follow the trend of larger particles leading to larger resistance per unit length. Resistivity from intergranular tunnelling can be generally described as

$$\rho \propto (1 + P^2m^2)^{-1} \exp\left(\sqrt{\frac{2\kappa C}{kT}}\right) \quad (2)$$

where P is the spin polarization, m is the reduced magnetization, κ is a tunnelling constant, C is a charging energy, and k is the Boltzmann constant.[35] The $(1 + P^2m^2)^{-1}$ factor determines the magnetoresistance, while the $\exp(\sqrt{2\kappa C/kT})$ factor determines the overall tunnelling rate. In our samples, the tunnelling rate should be determined primarily by the charging energy. The tunnelling constant κ depends on barrier height and width, as well as intrinsic material properties, which are invariant across the four $CoFe_2O_4$ samples. However, the charging energy should decrease significantly as the size of the nanoparticles increases, explaining the decreasing resistivity with nanoparticle size observed.

In the course of our study, one sample of $CoFe_2O_4$ (d = 12.9 nm) was discovered to display wholly anomalous MR behavior. Despite size, compositional, and magnetic similarity (Figure S7), these particles were synthesized to have an octahedral habit. Temperature-dependence of their resistance lacks the characteristic ln $R \propto T^{-0.5}$ relationship, and the magnitude of the resistance is orders of magnitude lower than that of our other $CoFe_2O_4$ and Fe_3O_4 samples. In fact, the temperature-dependence shown in Figure 4 looks like that of a bulk

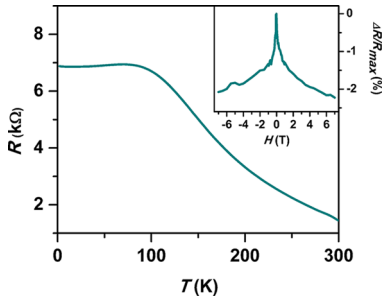

Figure 4. Temperature-dependence of the resistance of octahedrally faceted d = 12.9 nm $CoFe_2O_4$ nanoparticles. Inset: room temperature magnetoresistance behavior of the same nanoparticles.

semiconductor, with an intrinsic region from about 100 to 300 K and an extrinsic region below 100 K. The greatly decreased resistance of the sample supports the idea that it is behaving as a bulk semiconductor. The truncated octahedral form, lack of bulky ligands, and pressure applied during pellet formation could promote enhanced contact between nanoparticles along matching crystal facets. Fusing of faceted nanoparticles upon ligand removal has been observed in the literature.[37,38] Although discrete particles are still distinguishable by scanning electron microscopy (Figure S8), the interfacing of some crystal planes between nanoparticles could provide increased wave function overlap between particles, forming a conductive pathway and eliminating the TMR effect. Charge carriers are able to conduct through this sample similarly to bulk material, rather than by tunnelling between individual nanoparticles. In other applications requiring high conductivity in nanoparticle solids, this mechanism could provide a new materials processing strategy. The decreased $\Delta R/R$ of the 12.9 nm pellet (maximum $\Delta R/R$ = 2.2%) compared to the other $CoFe_2O_4$ samples demonstrates the importance of tunnelling barriers and TMR to strong granular MR.

In this work we have performed the first analysis of the importance of size on the strength of nanoparticle granular MR. Our results demonstrate that the size regime of the particle, more than any specific magnetic parameter, determines the strength of the MR effect. In fact, magnetic ordering or superparamagnetic blocking are not required—thus opening the door to a much wider range of potential MR materials that have remained unexplored. Additionally, it was determined that $CoFe_2O_4$ nanoparticles have comparable or favorable MR values when compared to Fe_3O_4. Despite the status of Fe_3O_4 as the material of choice in the field, owing to its high predicted spin polarization, the (d = 8.4 nm) $CoFe_2O_4$ nanoparticles showed a higher room temperature maximum $\Delta R/R$ of 18.4%, compared to 10.8% for similarly sized Fe_3O_4. These data help demonstrate the value of colloidal synthesis to this field, allowing for wide-ranging and inexpensive exploration of materials with well-defined composition and size in a way that is not possible by traditional top-down methods. Although the methods employed here lack the atomic precision of traditional multilayer thin films, the sheer number of junctions drastically enhances the chances of an observable effect. This both allows for simple screening conditions and

DOI: 10.1021/acscentsci.8b00399
ACS Cent. Sci. 2018, 4, 1222−1227

suggests that optimization of promising materials could result in drastic improvements.

■ ASSOCIATED CONTENT

Supporting Information

The Supporting Information is available free of charge on the ACS Publications website at DOI: 10.1021/acscentsci.8b00399.

Experimental details, pXRD patterns, additional TEM and SEM images, temperature- and field-dependent magnetism and magnetoresistance of Fe_3O_4 nanoparticles, low-temperature magnetoresistance curves of $CoFe_2O_4$ nanoparticles, and a summary of magnetic parameters for each nanoparticle sample (PDF)

■ AUTHOR INFORMATION

Corresponding Author

*E-mail: jrinehart@ucsd.edu.

ORCID

Benjamin H. Zhou: 0000-0003-1018-5929

Jeffrey D. Rinehart: 0000-0002-5478-1995

Notes

The authors declare no competing financial interest.

■ ACKNOWLEDGMENTS

This research was funded through the Office of Naval Research Young Investigator Award N00014-16-1-2917. This work was performed in part at the San Diego Nanotechnology Infrastructure (SDNI) of UCSD, a member of the National Nanotechnology Coordinated Infrastructure, which is supported by the National Science Foundation (Grant ECCS-1542148). We also thank Dr. Milan Gembicky for his assistance with powder X-ray diffraction measurements. J.D.R. would like to express deep gratitude for the enthusiasm, inspiration, and wisdom of Prof. Ami E. Berkowitz.

■ REFERENCES

(1) Baibich, M. N.; Broto, J. M.; Fert, A.; Vandau, F. N.; Petroff, F.; Eitenne, P.; Creuzet, G.; Friederich, A.; Chazelas, J. Giant magnetoresistance of (001)Fe/(001)Cr magnetic superlattices. *Phys. Rev. Lett.* **1988**, *61* (21), 2472.

(2) Binasch, G.; Grunberg, P.; Saurenbach, F.; Zinn, W. Enhanced magnetoresistance in layered magnetic-structures with antiferromagnetic interlayer exchange. *Phys. Rev. B: Condens. Matter Mater. Phys.* **1989**, *39* (7), 4828.

(3) Pannetier-Lecoeur, M.; Fermon, C.; de Vismes, A.; Kerr, E.; Vieux-Rochaz, L. Low noise magnetoresistive sensors for current measurement and compasses. *J. Magn. Magn. Mater.* **2007**, *316* (2), e246.

(4) Michelena, M. D.; Oelschlägel, W.; Arruego, I.; del Real, R. P.; Mateos, J. A. D.; Merayo, J. M. Magnetic giant magnetoresistance commercial off the shelf for space applications. *J. Appl. Phys.* **2008**, *103* (7), 07e912.

(5) Chiang, C.-Y.; Jeng, J.-T.; Lai, B.-L.; Luong, V. S.; Lu, C.-C. Triaxis magnetometer with in-plane giant magnetoresistance sensors for compass application. *J. Appl. Phys.* **2015**, *117* (17), 17a321.

(6) Issadore, D.; Park, Y. I.; Shao, H.; Min, C.; Lee, K.; Liong, M.; Weissleder, R.; Lee, H. Magnetic sensing technology for molecular analyses. *Lab Chip* **2014**, *14* (14), 2385.

(7) Martins, V. C.; Cardoso, F. A.; Germano, J.; Cardoso, S.; Sousa, L.; Piedade, M.; Freitas, P. P.; Fonseca, L. P. Femtomolar limit of detection with a magnetoresistive biochip. *Biosens. Bioelectron.* **2009**, *24* (8), 2690.

(8) Gaster, R. S.; Xu, L.; Han, S.-J.; Wilson, R. J.; Hall, D. A.; Osterfeld, S. J.; Yu, H.; Wang, S. X. Quantification of protein interactions and solution transport using high-density GMR sensor arrays. *Nat. Nanotechnol.* **2011**, *6* (5), 314.

(9) Huang, C. C.; Zhou, X.; Hall, D. A. Giant magnetoresistive biosensors for time-domain magnetorelaxometry: A theoretical investigation and progress toward an immunoassay. *Sci. Rep.* **2017**, *7*, 45493.

(10) Lange, J.; Kotitz, R.; Haller, A.; Trahms, L.; Semmler, W.; Weitschies, W. Magnetorelaxometry - a new binding specific detection method based on magnetic nanoparticles. *J. Magn. Magn. Mater.* **2002**, *252* (1−3), 381.

(11) Dogaru, T.; Smith, S. T. Giant magnetoresistance-based eddy-current sensor. *IEEE Trans. Magn.* **2001**, *37* (5), 3831.

(12) Pelkner, M.; Neubauer, A.; Reimund, V.; Kreutzbruck, M.; Schütze, A. Routes for GMR-sensor design in non-destructive testing. *Sensors* **2012**, *12* (9), 12169.

(13) Sahoo, D. R.; Sebastian, A.; Häberle, W.; Pozidis, H.; Eleftheriou, E. Scanning probe microscopy based on magnetoresistive sensing. *Nanotechnology* **2011**, *22* (14), 145501.

(14) Berkowitz, A. E.; Mitchell, J. R.; Carey, M. J.; Young, A. P.; Zhang, S.; Spada, F. E.; Parker, F. T.; Hutten, A.; Thomas, G. Giant magnetoresistance in heterogeneous Cu-Co alloys. *Phys. Rev. Lett.* **1992**, *68* (25), 3745.

(15) Xiao, J. Q.; Jiang, J. S.; Chien, C. L. Giant magnetoresistance in nonmultilayer magnetic systems. *Phys. Rev. Lett.* **1992**, *68* (25), 3749.

(16) Schneider, C. A.; Rasband, W. S.; Eliceiri, K. W. NIH Image to ImageJ: 25 years of image analysis. *Nat. Methods* **2012**, *9* (7), 671.

(17) Coey, J. M. D.; Berkowitz, A. E.; Balcells, L.; Putris, F. F.; Parker, F. T. Magnetoresistance of magnetite. *Appl. Phys. Lett.* **1998**, *72* (6), 734.

(18) Mitra, A.; Barick, B.; Mohapatra, J.; Sharma, H.; Meena, S. S.; Aslam, M. Large tunneling magnetoresistance in octahedral Fe_3O_4 nanoparticles. *AIP Adv.* **2016**, *6* (5), 055007.

(19) Lv, Z. P.; Luan, Z. Z.; Cai, P. Y.; Wang, T.; Li, C. H.; Wu, D.; Zuo, J. L.; Sun, S. H. Enhancing magnetoresistance in tetrathiafulvalene carboxylate modified iron oxide nanoparticle assemblies. *Nanoscale* **2016**, *8* (24), 12128.

(20) Lv, Z. P.; Luan, Z. Z.; Wang, H. Y.; Liu, S.; Li, C. H.; Wu, D.; Zuo, J. L.; Sun, S. H. Tuning electron-conduction and spin transport in magnetic iron oxide nanoparticle assemblies via tetrathiafulvalene-fused ligands. *ACS Nano* **2015**, *9* (12), 12205.

(21) Wang, S.; Yue, F. J.; Wu, D.; Zhang, F. M.; Zhong, W.; Du, Y. W. Enhanced magnetoresistance in self-assembled monolayer of oleic acid molecules on Fe_3O_4 nanoparticles. *Appl. Phys. Lett.* **2009**, *94* (1), 012507.

(22) Wang, W.; Yu, M.; Batzill, M.; He, J.; Diebold, U.; Tang, J. Enhanced tunneling magnetoresistance and high-spin polarization at room temperature in a polystyrene-coated Fe_3O_4 granular system. *Phys. Rev. B: Condens. Matter Mater. Phys.* **2006**, *73* (13), 134412.

(23) Liu, K.; Zhao, L.; Klavins, P.; Osterloh, F. E.; Hiramatsu, H. Extrinsic magnetoresistance in magnetite nanoparticles. *J. Appl. Phys.* **2003**, *93* (10), 7951.

(24) Kohiki, S.; Kinoshita, T.; Nara, K.; Akiyama-Hasegawa, K.; Mitome, M. Large, negative magnetoresistance in an oleic acid-coated Fe_3O_4 nanocrystal self-assembled film. *ACS Appl. Mater. Interfaces* **2013**, *5* (22), 11584.

(25) Kohiki, S.; Okada, K.; Mitome, M.; Kohno, A.; Kinoshita, T.; Iyama, K.; Tsunawaki, F.; Deguchi, H. Magnetic and magnetoelectric properties of self-assembled $Fe_{2.5}Mn_{0.5}O_4$ nanocrystals. *ACS Appl. Mater. Interfaces* **2011**, *3* (9), 3589.

(26) Poddar, P.; Fried, T.; Markovich, G. First-order metal-insulator transition and spin-polarized tunneling in Fe_3O_4 nanocrystals. *Phys. Rev. B: Condens. Matter Mater. Phys.* **2002**, *65* (17), 172405.

(27) Zeng, H.; Black, C. T.; Sandstrom, R. L.; Rice, P. M.; Murray, C. B.; Sun, S. Magnetotransport of magnetite nanoparticle arrays. *Phys. Rev. B: Condens. Matter Mater. Phys.* **2006**, *73* (2), 020402.

(28) Lv, Z.-P.; Wang, T.; Ge, J.-Y.; Luan, Z.-Z.; Wu, D.; Zuo, J.-L.; Sun, S. Controlling the assembly and spin transport of tetrathiafulva-

DOI: 10.1021/acscentsci.8b00399
ACS Cent. Sci. 2018, 4, 1222−1227

lene carboxylate coated iron oxide nanoparticles. *J. Mater. Chem. C* **2017**, *5* (29), 7200.
(29) Kohiki, S.; Nara, K.; Mitome, M.; Tsuya, D. Magnetoresistance of drop-cast film of cobalt-substituted magnetite nanocrystals. *ACS Appl. Mater. Interfaces* **2014**, *6* (20), 17410.
(30) Chen, J.; Ye, X.; Oh, S. J.; Kikkawa, J. M.; Kagan, C. R.; Murray, C. B. Bistable magnetoresistance switching in exchange-coupled $CoFe_2O_4$-Fe_3O_4 binary nanocrystal superlattices by self-assembly and thermal annealing. *ACS Nano* **2013**, *7* (2), 1478.
(31) Anil Kumar, P.; Ray, S.; Chakraverty, S.; Sarma, D. D. Engineered spin-valve type magnetoresistance in Fe_3O_4-$CoFe_2O_4$ core-shell nanoparticles. *Appl. Phys. Lett.* **2013**, *103* (10), 102406.
(32) Sun, S.; Zeng, H.; Robinson, D. B.; Raoux, S.; Rice, P. M.; Wang, S. X.; Li, G. Monodisperse MFe_2O_4 (M = Fe, Co, Mn) nanoparticles. *J. Am. Chem. Soc.* **2004**, *126* (1), 273.
(33) Yu, Y.; Mendoza-Garcia, A.; Ning, B.; Sun, S. Cobalt-substituted magnetite nanoparticles and their assembly into ferrimagnetic nanoparticle arrays. *Adv. Mater.* **2013**, *25* (22), 3090.
(34) Dong, A.; Ye, X.; Chen, J.; Kang, Y.; Gordon, T.; Kikkawa, J. M.; Murray, C. B. A generalized ligand-exchange strategy enabling sequential surface functionalization of colloidal nanocrystals. *J. Am. Chem. Soc.* **2011**, *133* (4), 998.
(35) Inoue, J.; Maekawa, S. Theory of tunneling magnetoresistance in granular magnetic films. *Phys. Rev. B: Condens. Matter Mater. Phys.* **1996**, *53* (18), R11927.
(36) Zabet-Khosousi, A.; Dhirani, A. A. Charge transport in nanoparticle assemblies. *Chem. Rev.* **2008**, *108* (10), 4072.
(37) Robinson, E. H.; Turo, M. J.; Macdonald, J. E. Controlled surface chemistry for the directed attachment of copper(I) sulfide nanocrystals. *Chem. Mater.* **2017**, *29* (9), 3854.
(38) Gupta, S.; Wu, W.-Y.; Chakrabortty, S.; Li, M.; Wang, Y.; Ong, X.; Chan, Y. Hierarchical multicomponent nanoheterostructures via facet-to-facet attachment of anisotropic semiconductor nanoparticles. *Chem. Mater.* **2017**, *29* (21), 9075.

DOI: 10.1021/acscentsci.8b00399
ACS Cent. Sci. 2018, 4, 1222−1227